PHYSICAL REVIEW B **102**, 224103 (2020)

Temperature-induced structural evolution in liquid Ag-Ga alloys

Yu Su,[1] Xiaodong Wang,[1,*] Yang Ren,[2] Qingping Cao,[1] Dongxian Zhang,[1,3] and Jian-Zhong Jiang[1,†]
[1]*International Center for New-Structured Materials (ICNSM), Laboratory of New-Structured Materials, State Key Laboratory of Silicon Materials, and School of Materials Science and Engineering, Zhejiang University, Hangzhou 310027, People's Republic of China*
[2]*Advanced Photon Source, Argonne National Laboratory, Argonne, Illinois 60439, USA*
[3]*State Key Laboratory of Modern Optical Instrumentation, Zhejiang University, Hangzhou 310027, People's Republic of China*

(Received 22 September 2020; revised 30 November 2020; accepted 3 December 2020; published 18 December 2020)

Temperature-dependent atomic structural evolutions of liquid $Ag_{60}Ga_{40}$ and $Ag_{70}Ga_{30}$ alloys have been studied by *in situ* high-energy x-ray-diffraction (HEXRD) experiments combined with *ab initio* molecular-dynamics simulations. The experimental data show a reversible structural crossover at about $1050 \sim 1100$ (± 50) K in both liquid $Ag_{60}Ga_{40}$ and $Ag_{70}Ga_{30}$ alloys. Obvious changes of the electrical resistivity, absolute thermoelectric power, and atomic diffusivity around the similar temperature range for both Ag-Ga liquids strongly support the HEXRD results. The origin of the liquid-to-liquid crossover in both Ag-Ga liquids was suggested to link with the rearrangements of Ag and Ga atoms, i.e., Ag and Ga atoms prefer to associate with themselves in the higher temperature range above 1100 K, consistent with the accelerated increase of the strong covalently bonded Ga–Ga dimers in both Ag-Ga liquids. In addition, more studies from the energy aspect are still desirable to understand the rearrangements of Ag and Ga atoms in the higher temperature range in both Ag-Ga liquids.

DOI: 10.1103/PhysRevB.102.224103

I. INTRODUCTION

Metallic glasses (MGs) have received considerable attention due to their unique disordered atomic-packing structures and excellent mechanical, magnetic, corrosion, and superelastic deformation properties. Since most MGs are fabricated by rapidly quenching from their corresponding melts, they are sometimes termed as frozen liquids. Hence, tracking the structural evolutions of metallic liquids with temperature cannot only deepen the understanding of the glass formation, but also uncover the novel phenomena in the liquids. For example, intensive investigations demonstrate that temperature-induced liquid-to-liquid phase transition (LLPT) could exist in some monoatomic metallic liquids, e.g., Ce [1,2], Cs [2], Ga [2,3], Si [4], Rb [5], binary metallic liquids, e.g., $Ga_{85.8}In_{14.2}$ [6], $In_{80}Sn_{20}$ [7,8], $Sn_{85}Zn_{15}$ [9], $Pb_{26}Sn_{74}$ [10], and multicomponent metallic liquids, e.g., $La_{50}Al_{35}Ni_{15}$ [11], $Pd_{41.25}Ni_{41.25}P_{17.5}$ [12], and $Zr_{41.2}Ti_{13.8}Cu_{12.5}Ni_{10}Be_{22.5}$ [13]. In addition, metallic liquids of noble metals with polyvalent elements usually show nonlinear properties with temperatures [14–24], including the silver-gallium (Ag-Ga) system, in which nonlinear changes in the electrical resistivity and absolute thermoelectric power were found as a function of temperature. Shirakawa *et al.* [25] further studied the thermodynamic stability of Ag-polyvalent metallic liquids, and the concentration-concentration fluctuation in long-wavelength limit $S_{cc}(0)$ shows some ordered states on the Ag-rich side, which most likely originate from the rigid electronic density of states of Ag atoms. Kaban and Hoyer [26] assumed the coexistence of electronically stabilized clusters and clusters of pure elements (either noble or polyvalent metal depending on the concentration of the alloys) in noble-polyvalent metallic liquids, which are caused by the topological and chemical short-range ordering in the liquid state. However, due to the lack of solid structural evidence from advanced experimental techniques, e.g., *in situ* high-energy x-ray diffraction (HEXRD), and theoretical analysis methods, e.g., *ab initio* molecular-dynamics (AIMD) simulations, whether the anomalous structural evolution, e.g., the LLPT, exists in noble-polyvalent metallic systems is still uncertain. Here we selected the Ag-Ga system, as a prototype of noble-polyvalent metallic alloys, to investigate the possible temperature-induced structural changes in the Ag-Ga liquids via *in situ* HEXRD experiments and AIMD simulations. All obtained experimental and theoretical results reveal reversible structural crossovers at about $1050 \sim 1100$ (± 50) K in both liquid $Ag_{60}Ga_{40}$ and $Ag_{70}Ga_{30}$ alloys, leading to deviations from the linear evolutions of the first two peaks on the structure factor $S(q)$, reduced pair-distribution function $G(r)$, partial coordination numbers (CNs), and covalently bonded Ga–Ga dimers. Properties, e.g., atomic diffusivity, electrical resistivity, and absolute thermoelectric power, can also be affected by appearing kinks around the similar temperature range. These findings in noble-polyvalent metallic liquids will trigger more studies on the temperature-dependent local structural evolutions in other metallic liquids.

II. METHODS

A. *In situ* HEXRD experiments

The $Ag_{60}Ga_{40}$ and $Ag_{70}Ga_{30}$ (at. %) alloys were prepared by arc melting high-purity Ag (99.999%) and Ga (99.999%) slugs. The parent ingots were remelted for more than five times to ensure the chemical homogeneity. Then rods with

---

[*] wangxd@zju.edu.cn
[†] jiangjz@zju.edu.cn

©2020 American Physical Society

6-mm length cut from corresponding parent ingots were sealed into quartz capillaries with 1.5-mm diameter under a vacuum of about 4.6×10^{-4} Pa. *In situ* HEXRD experiments were carried out at the beamline 11-ID-C, Advanced Photon Source (APS), Chicago. The sealed samples were heated by a Linkam TS1500 furnace with a heating/cooling rate of 10 K/min and an effective temperature range of $850 \sim 1320$ K. The x-ray beam size used was about 0.5×0.5 mm^2 with a wavelength of 0.1173 Å (the x-ray energy was about 106 keV). The diffraction patterns were automatically collected by a flat-panel Si detector (PerkinElmer 1621) with 200×200-μm^2 pixel size and 2048×2048 pixels. The exposure time was 0.1 s and 200 diffraction patterns were summed for each dataset. The pattern from an empty capillary with the same diameter and exposure time was used as a background. High-quality scattering intensity $I(q)$ was integrated from two-dimensional diffraction patterns by using the software package FIT2D [27]. The standard procedures were carried out to extract the experimental $S(q)$ and $G(r)$ curves from $I(q)$ data after subtracting the appropriate background by using the software package PDFGETX3 [28]. Another structural analysis software, GSAS-II [29], was also applied to confirm the $S(q)$ and $G(r)$ curves obtained from PDFGETX3, showing a good agreement between them.

B. Computational details

AIMD simulations of liquid $Ag_{60}Ga_{40}$ and $Ag_{70}Ga_{30}$ alloys were accomplished based on the density-functional theory by using the Vienna *Ab initio* Simulation Package (VASP) [30]. The canonical NVT ensemble (i.e., constant atom number, volume, and temperature) was adopted during the AIMD simulations [31–34] and the Nosé-Hoover thermostat was applied to control the system temperature [35,36], combined with the projector augmented wave method [37]. The generalized gradient approximation of Perdew and Wang [37,38] was used to describe the interaction between electrons and ions. Newton's equations of motion were integrated with the velocity Verlet algorithm and a time interim of 3 fs. Only the Γ point was used to sample the Brillouin zone of the supercell. Cubic cells containing 200 atoms (120 Ag and 80 Ga atoms for liquid $Ag_{60}Ga_{40}$ alloy, while 140 Ag and 60 Ga atoms for liquid $Ag_{70}Ga_{30}$ alloy) with periodic boundary conditions were first constructed and relaxed at 1500 K (well above their melting points) for more than 8000 steps to remove the memory effect of the initial configurations, then experienced a stepwise quenching process at a cooling rate of 3.33×10^{13} K/s from 1500 to 700 K with the temperature interval of 100 K. At each temperature, the cell sizes were adjusted to make the average internal pressure close to zero within ±0.5 kbar. Afterward, another additional 6000 steps were carried out for the structural relaxation. The relaxed atomic configuration was recorded at each step, and then the subsequent structural information, e.g., $S(q)$ and $g(r)$, etc., were calculated by taking the average of the last 3000 configurations. Figures S1(a) and S1(b) in the Supplemental Material [39] exhibit the mean-square displacement (MSD) as a function of time at various temperatures from 700 to 1500 K for liquid $Ag_{60}Ga_{40}$ and $Ag_{70}Ga_{30}$ alloys, respectively. The positive evolutions of the MSD data manifest that both Ag-Ga alloys are in the liquid state with good mobility during the whole studied temperature range, even at 700 and 800 K below the liquidus temperatures (T_L) of $Ag_{60}Ga_{40}$ and $Ag_{70}Ga_{30}$ alloys of about 790 and 840 K, respectively [40]. Moreover, the nearly linear dependence of all the MSD curves with time indicates that the systems are in good equilibrium after 6000-step relaxation at each temperature, further confirming the reliability of the configurations obtained from AIMD simulations for all studied temperatures below and above the T_L.

III. RESULTS AND DISCUSSION

A. Structural analyses by *in situ* HEXRD experiments

Structure factors $S(q)$ of liquid $Ag_{60}Ga_{40}$ and $Ag_{70}Ga_{30}$ alloys obtained from the *in situ* HEXRD experiments upon heating are plotted in Figs. 1(a) and 1(b), respectively, while Figs. 1(c) and 1(d) show the temperature-dependent $G(r)$ curves of liquid $Ag_{60}Ga_{40}$ and $Ag_{70}Ga_{30}$ alloys, respectively, which can be derived by the Fourier transformation from $S(q)$ data. High quality of $S(q)$ and $G(r)$ curves ensures the reliability of the subsequent structural analyses based on these data. Considering the symmetrical peak profiles, we applied a Gaussian function with a linear baseline to fit the first two peaks of $S(q)$ and $G(r)$ curves, marked as q_1, q_2, r_1, and r_2, respectively [see Figs. 1(a)–1(d)]. Temperature-dependent evolutions of the peak positions of q_1, q_2, r_1, and r_2 on the $S(q)$ and $G(r)$ curves of liquid $Ag_{60}Ga_{40}$ alloy are plotted in Figs. 2(a)–2(d), respectively. The red open circles represent the heating procedure while the blue ones represent the cooling procedure. The peak positions of all these four peaks coincide well during the heating and cooling procedures, indicating that a reversible structural evolution happened in liquid $Ag_{60}Ga_{40}$ alloy. Moreover, the peak position of q_1 shifts to low-q side while the peak position of q_2 moves to high-q side as the temperature increases from 850 to 1320 K, indicating that although the whole liquid $Ag_{60}Ga_{40}$ alloy expands, its local atomic packing structure exists with some shrinkage with temperature. Not only here in liquid $Ag_{60}Ga_{40}$ alloy, this opposite temperature dependence of q_1 and q_2 is also experimentally observed in many monoatomic metallic liquids of Zn [41] and In [41], binary metallic liquids of $Au_{44}Ga_{56}$ [42], $Ga_{85.8}In_{14.2}$ [6], $Zr_{75.5}Pd_{24.5}$ [43], $Zr_{80}Pt_{20}$ [44], In-Sn [45], and $Al_{90}Sm_{10}$ [46], and multicomponent metallic liquids of $Pd_{43}Cu_{27}Ni_{10}P_{20}$ [47,48], $Pt_{42.5}Cu_{27}Ni_{9.5}P_{21}$ [48], $Zr_{57}Nb_5Al_{10}Cu_{15.4}Ni_{12.6}$ [49], and $Zr_{41.2}Ti_{13.8}Cu_{12.5}Ni_{10}Be_{22.5}$ [13]. If checking the evolutions of r_1 and r_2 on $G(r)$ curves [see Figs. 2(c) and 2(d), respectively], it is found that this local shrinkage originates from r_1, i.e., the nearest-neighboring distances in clusters between the central atoms and atoms at the first shell shrink with the increase of the temperature. The "contradiction behavior" between the temperature-dependent evolutions of q_1 and r_1 is due to the different correlation lengths of these two peaks. One could generally consider that q_1 on $S(q)$ is linked with the liquid density, i.e., the lower the peak position, the lower the density, and the expansion of the whole liquid upon heating leads to the decrease of the density as well as the peak position of q_1. However, r_1 on $G(r)$ reveals only the local atomic packings (relative high scattering of x ray in denser atomic clusters) in

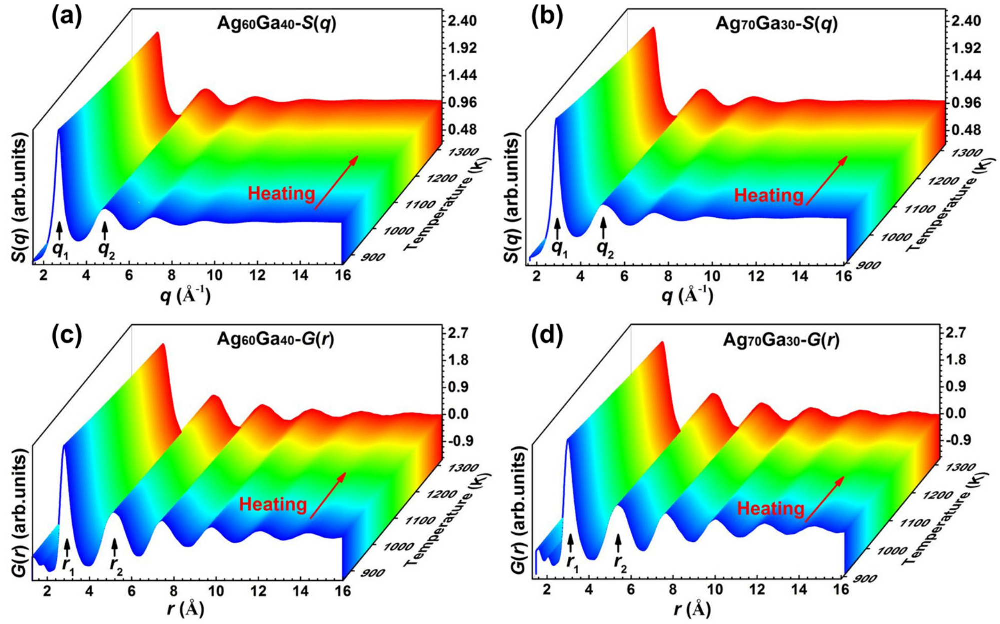

FIG. 1. (a), (b) Waterfall graphs of the high-quality $S(q)$ curves of liquid $Ag_{60}Ga_{40}$ and $Ag_{70}Ga_{30}$ alloys, respectively, obtained from *in situ* HEXRD experiments for the heating procedure. (c), (d) Waterfall graphs of the high-quality $G(r)$ curves of liquid $Ag_{60}Ga_{40}$ and $Ag_{70}Ga_{30}$ alloys, respectively, obtained from *in situ* HEXRD experiments for the heating procedure.

short range (less than 4 Å), and the x-ray scattering power from the free-volume part induced by temperature between clusters in metallic liquids is much weaker as compared to the denser atomic clusters. A general picture for this negative expansion phenomenon on the first shell of $G(r)$ in metallic liquids has been given by Lou *et al.* [50]. Beyond the single cluster, r_2 on $G(r)$ is usually closely related to the connection between various clusters [41,51,52], and the expansion

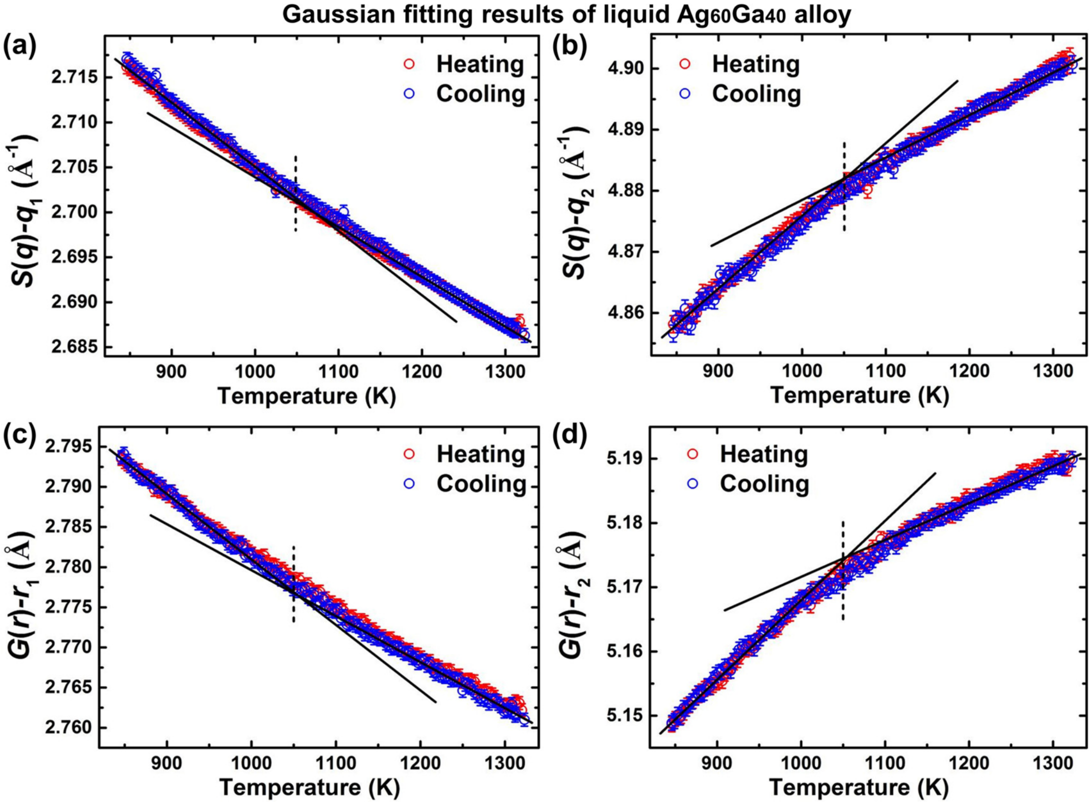

FIG. 2. (a)–(d) Peak positions of the first two peaks on the experimental $S(q)$ and $G(r)$ curves of liquid $Ag_{60}Ga_{40}$ alloy as a function of temperature, marked as q_1, q_2, r_1, and r_2, respectively. The red open circles represent the heating procedure while the blue open circles represent the cooling procedure.

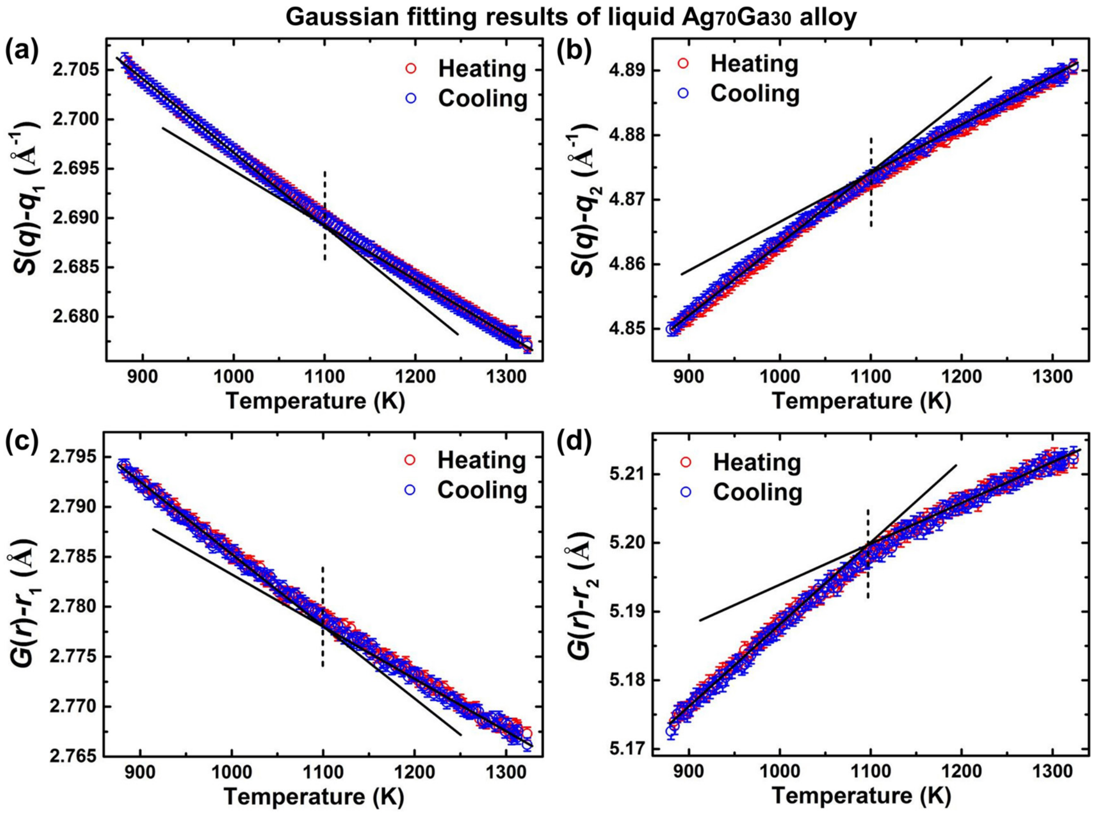

FIG. 3. (a)–(d) Peak positions of the first two peaks on the experimental $S(q)$ and $G(r)$ curves of liquid $Ag_{70}Ga_{30}$ alloy as a function of temperature, marked as q_1, q_2, r_1, and r_2, respectively. The red open circles represent the heating procedure while the blue open circles represent the cooling procedure.

behavior of r_2 suggests the formation of more free volumes between different atomic clusters upon heating, which enlarge the distances between clusters and reduce the densities of these cluster associations. In addition, guided by the trend lines in Figs. 2(a)–2(d), it is noteworthy that the peak positions of all four peaks of q_1, q_2, r_1, and r_2 deviate from the linear feature at about 1050 ± 50 K, indicating that there might exist some kinds of structural changes in short and/or medium ranges below and above 1050 ± 50 K in liquid $Ag_{60}Ga_{40}$ alloy. To verify the reliability of the Gaussian fittings, we directly capture the maxima of the $S(q)$ and $G(r)$ peaks, and Figs. S2(a) and S2(b) in the Supplemental Material [39] display the temperature-dependent evolutions of the maxima of q_1 and r_1 on $S(q)$ and $G(r)$ curves of liquid $Ag_{60}Ga_{40}$ alloy, respectively. It is found that except for slight shifts of the exact values, both evolutions of q_1 and r_1 derived by taking the maxima directly exhibit the similar tendencies with temperature, and also deviate from linearity at about 1050 ± 50 K, confirming that using the Gaussian functions to fit both $S(q)$ and $G(r)$ peaks is reliable. Figures 3(a)–3(d) display the temperature-dependent evolutions of the peak positions of q_1, q_2, r_1, and r_2, respectively, on the $S(q)$ and $G(r)$ curves of liquid $Ag_{70}Ga_{30}$ alloy. The evolutions of all four peaks with temperature show similar tendencies with those of liquid $Ag_{60}Ga_{40}$ alloy shown in Figs. 2(a)–2(d), indicating an expansion behavior of the whole liquid $Ag_{70}Ga_{30}$ alloy and some shrinkage in short-range structures with the increase of the temperature. Moreover, guided by the trend lines in Figs. 3(a)–3(d), the peak positions of all four peaks of liquid $Ag_{70}Ga_{30}$ alloy also deviate from the linear feature at about 1100 ± 50 K, which is reversible, indicating the existence of some kinds of structural changes in short and/or medium ranges in liquid $Ag_{70}Ga_{30}$ alloy below and above 1100 ± 50 K. However, more evidence is strongly desirable to support the structural crossovers observed by *in situ* HEXRD experiments in liquid $Ag_{60}Ga_{40}$ and $Ag_{70}Ga_{30}$ alloys.

B. Structural analyses by AIMD simulations

To track the local structural evolutions and dynamical properties of liquid $Ag_{60}Ga_{40}$ and $Ag_{70}Ga_{30}$ alloys, AIMD simulations were carried out which could provide the underlying mechanism for above findings obtained from *in situ* HEXRD experiments. The reliability of the atomic configurations produced by the VASP package for metallic liquids has been proved by previous literature [3,6,9,42,53–59]. Moreover, the open circles in Fig. 4 display the simulated $S(q)$ and the pair-correlation function $g(r)$ of liquid $Ag_{60}Ga_{40}$ and $Ag_{70}Ga_{30}$ alloys at various temperatures from 700 to 1500 K, while the colored curves represent the $S(q)$ and $g(r)$ data obtained from *in situ* HEXRD experiments at corresponding temperatures. The experimental $g(r)$ can be deduced by the following equation:

$$g(r) = 1 + \frac{G(r)}{4\pi r\rho}, \tag{1}$$

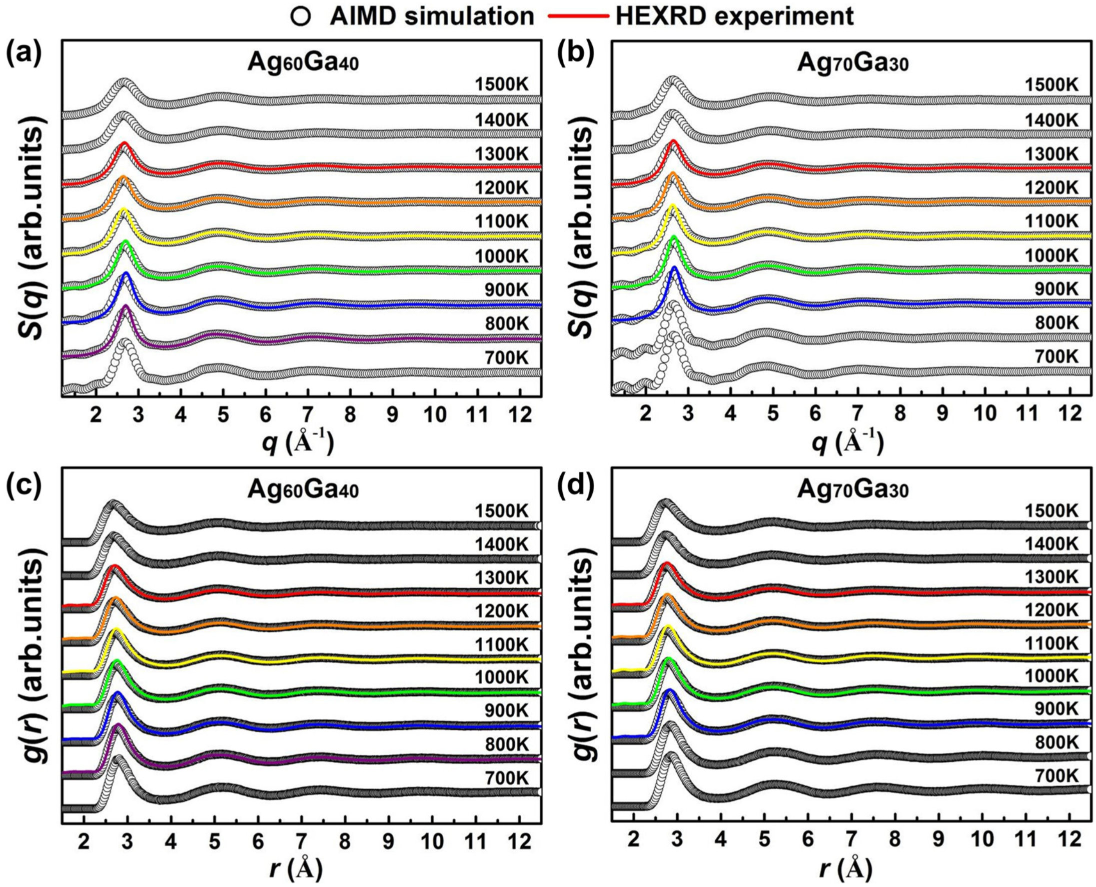

FIG. 4. (a), (b) Comparisons of the simulated $S(q)$ curves (open circles) and the corresponding experimental $S(q)$ data (colored curves) at various temperatures from 700 to 1500 K for liquid $Ag_{60}Ga_{40}$ and $Ag_{70}Ga_{30}$ alloys, respectively. (c), (d) Comparisons of the simulated $g(r)$ curves (open circles) and the corresponding experimental $g(r)$ data (colored curves) at various temperatures from 700 to 1500 K for liquid $Ag_{60}Ga_{40}$ and $Ag_{70}Ga_{30}$ alloys, respectively.

where ρ is the number density. The simulated $S(q)$ and $g(r)$ match well with the corresponding experimental data in terms of shape, peak position, etc., indicating that the atomic configurations produced by AIMD simulations could be reliable to capture the main structures of both liquid $Ag_{60}Ga_{40}$ and $Ag_{70}Ga_{30}$ alloys. The coordination number (CN), especially the nearest-neighboring atoms, is an important indicator to reflect the local atomic-packing structures of metallic liquids on the short-range scale. Based on these atomic configurations, we analyzed the temperature-dependent evolutions of the nearest-neighboring CNs by using the Voronoi tessellation methods [60,61], which divide the three-dimensional space around a central atom into a particular polyhedral cell within a proper cutoff. These cells are recorded by the Voronoi index $\langle n_3, n_4, n_5, \ldots n_i \rangle$, where n_i is the number of i-edged polygons. The sum of n_i is equivalent to the nearest-neighboring CN around a central atom. The cutoff values chosen here were estimated at the minimum position of the right side of the first peak of simulated $g(r)$, i.e., 3.78 Å for liquid $Ag_{60}Ga_{40}$ alloy and 3.95 Å for liquid $Ag_{70}Ga_{30}$ alloy. The black spheres in Fig. 5(a) illustrate the evolution of the total CN of liquid $Ag_{60}Ga_{40}$ alloy as a function of temperature, which first decreases with the increase of the temperature, and deviates from the linearity at about 1000 ∼ 1100 K, as guided by the trend lines. Figure 5(a) also displays the temperature-dependent evolutions of the experimental CN during the heating (red open circles) and cooling (blue open circles) procedures, which could be obtained by integrating the first peak of the radial distribution function (RDF) derived from $G(r)$ data by using the following equation:

$$\mathrm{RDF} = 4\pi r^2 \rho + r\mathrm{G}(r), \tag{2}$$

where ρ is the number density. High-quality RDF curves of liquid $Ag_{60}Ga_{40}$ and $Ag_{70}Ga_{30}$ alloys are shown in Figs. S3(a) and S3(b), respectively, in the Supplemental Material [39]. Interestingly, crossovers at about 1050 ± 50 K are also clearly detected on the temperature-dependent evolutions of the experimental CN of liquid $Ag_{60}Ga_{40}$ alloy, consistent with the result of AIMD simulations. Although it is very hard to experimentally obtain the partial $G(r)$ and therefore for the partial CNs, AIMD simulations can easily estimate these structural parameters from the constructed atomic configurations at various temperatures. Figure 5(b) exhibits the partial CNs of $CN_{\text{Ag-Ag}}$, $CN_{\text{Ag-Ga}}$, $CN_{\text{Ga-Ag}}$, and $CN_{\text{Ga-Ga}}$ as a function of temperature for liquid $Ag_{60}Ga_{40}$ alloy. Kinks at about 1000 ∼ 1100 K can also be clearly detected on the evolutions of all these four partial CNs, in which partial $CN_{\text{Ag-Ga}}$ and $CN_{\text{Ga-Ag}}$ are first to decrease slowly from 5.14 to 4.97 and from 7.62 to 7.41, respectively, in the lower temperature range from 700 to 1000 K. However, with a further increase of the

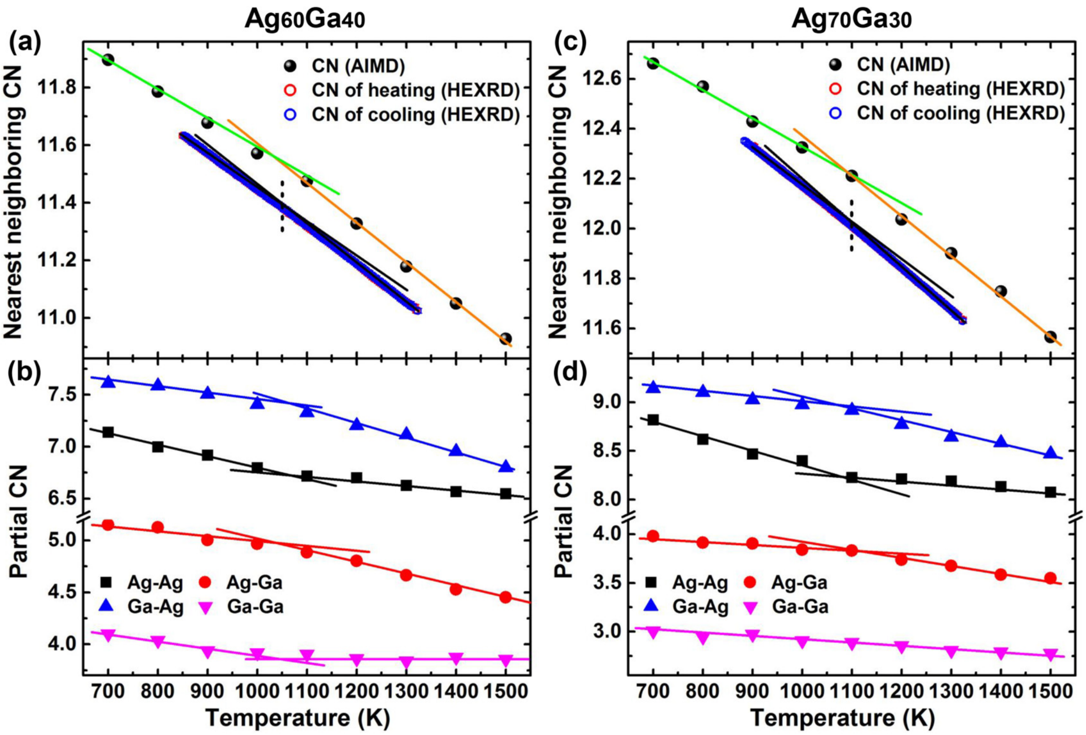

FIG. 5. (a), (c) The total nearest-neighboring CNs of liquid $Ag_{60}Ga_{40}$ and $Ag_{70}Ga_{30}$ alloys, respectively, as a function of temperature. The black spheres represent the CNs obtained from the Voronoi tessellation methods, and the open circles are the experimental data obtained from the RDF curves. (b), (d) The temperature-dependent evolutions of partial $CN_{Ag\text{-}Ag}$, $CN_{Ag\text{-}Ga}$, $CN_{Ga\text{-}Ag}$, and $CN_{Ga\text{-}Ga}$ in liquid $Ag_{60}Ga_{40}$ and $Ag_{70}Ga_{30}$ alloys, respectively.

temperature up to 1500 K, partial $CN_{Ag\text{-}Ga}$ and $CN_{Ga\text{-}Ag}$ show an accelerated decrease. On the contrary, partial $CN_{Ag\text{-}Ag}$ and $CN_{Ga\text{-}Ga}$ exhibit a relatively slower decrease in the higher temperature range from 1100 to 1500 K compared to that in the lower temperature range. These results suggest a repulsive interaction between Ag and Ga atoms in liquid $Ag_{60}Ga_{40}$ alloy; in other words, Ag atoms prefer to gather with Ag atoms while Ga atoms prefer to gather with Ga atoms in the higher temperature range, resulting in clear kinks at about $1000 \sim 1100$ K in the evolutions of total and partial CNs of liquid $Ag_{60}Ga_{40}$ alloy. Figure 5(c) shows the temperature-dependent evolutions of the total CN of liquid $Ag_{70}Ga_{30}$ alloy deduced from both HEXRD experiments and AIMD simulations, which show a similar tendency with temperature and deviate from the linearity at about 1100 ± 50 K, as guided by the trend lines in Fig. 5(c). By a careful check of the evolutions of partial CNs of liquid $Ag_{70}Ga_{30}$ alloy shown in Fig. 5(d), it is found that the partial CNs of $CN_{Ag\text{-}Ag}$, $CN_{Ag\text{-}Ga}$, and $CN_{Ga\text{-}Ag}$ also show clear kinks at about 1100 K. Similar to liquid $Ag_{60}Ga_{40}$ alloy, partial $CN_{Ag\text{-}Ga}$ and $CN_{Ga\text{-}Ag}$ of liquid $Ag_{70}Ga_{30}$ alloy exhibit an accelerated decrease while partial $CN_{Ag\text{-}Ag}$ appears to decrease much more slowly in the higher temperature range above 1100 K, again indicating a rearrangement of Ag and Ga atoms in liquid $Ag_{70}Ga_{30}$ alloy, in which Ag and Ga atoms prefer to associate with themselves at higher temperatures. However, there arises a question: Why do the Ag and Ga atoms with negative heat of mixing [62] trend to associate with themselves in the higher temperature range, rather than gather with each other? Note that liquid Ga behaves with both covalent and metallic characteristics, and

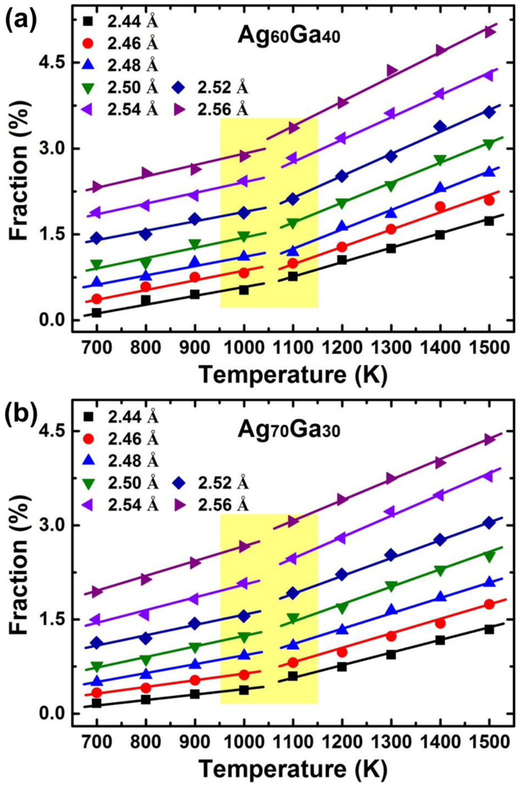

FIG. 6. The fractions of covalently bonded Ga–Ga dimers with temperature in liquid (a) $Ag_{60}Ga_{40}$ and (b) $Ag_{70}Ga_{30}$ alloys, respectively, by using different cutoff values from 2.44 to 2.56 Å.

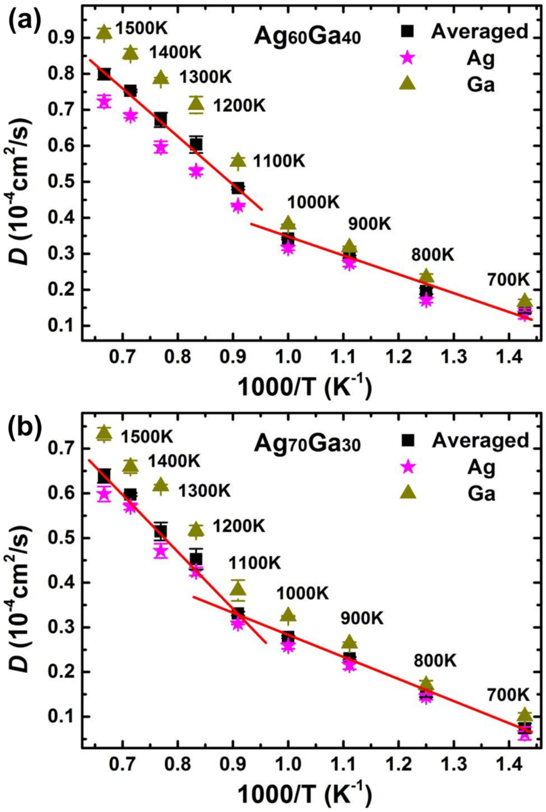

FIG. 7. Temperature-dependent self-diffusion coefficients (D) for the averaged, Ag and Ga atoms in liquid (a) $Ag_{60}Ga_{40}$ and (b) $Ag_{70}Ga_{30}$ alloys, respectively, obtained from AIMD simulations.

there exist strong covalently bonded Ga–Ga dimers which are the atomic pairs with the CN = 1 within a proper cutoff; we statistically counted the Ga atoms with only one neighbor Ga atom within a given cutoff value in both liquid $Ag_{60}Ga_{40}$ and $Ag_{70}Ga_{30}$ alloys. Considering that the interatomic distance of the covalently bonded Ga–Ga dimers is reported to be 2.484 Å in pure liquid Ga [3,63,64], different cutoff values around this from 2.44 to 2.56 Å were applied for both Ag-Ga liquids, as shown in Figs. 6(a) and 6(b), respectively. It is found that in both Ag-Ga liquids, no matter the cutoff selected, the fraction of Ga-Ga dimers first shows a slight increase upon heating from 700 to 1000 K. It then accelerates to go up when the temperature arises above 1100 K, implying that when the interactions among atoms in high-coordinated clusters are gradually broken by the thermal oscillation, the free Ga atoms in both Ag-Ga liquids prefer to gather with themselves to form strong covalently bonded dimers in the higher temperature range above 1100 K, along with the unities among free Ag atoms, consistent with the analyses of partial CNs shown in Figs. 5(b) and 5(d). In addition, more studies from the energy aspect are still desirable to understand the rearrangements of Ag and Ga atoms in the higher temperature range in both Ag-Ga liquids.

C. Properties of liquid Ag-Ga alloys

The above results suggest a structural crossover at about 1050 ∼ 1100 (±50) K in both liquid $Ag_{60}Ga_{40}$ and $Ag_{70}Ga_{30}$ alloys, which can most likely affect their properties, e.g., diffusivity, electrical resistivity, and thermoelectric power. Figure 7(a) shows the self-diffusion coefficients (D) of the averaged, Ag and Ga atoms in liquid $Ag_{60}Ga_{40}$ alloy as a function of temperature, which could be derived from the MSD data by using the Stokes-Einstein equation

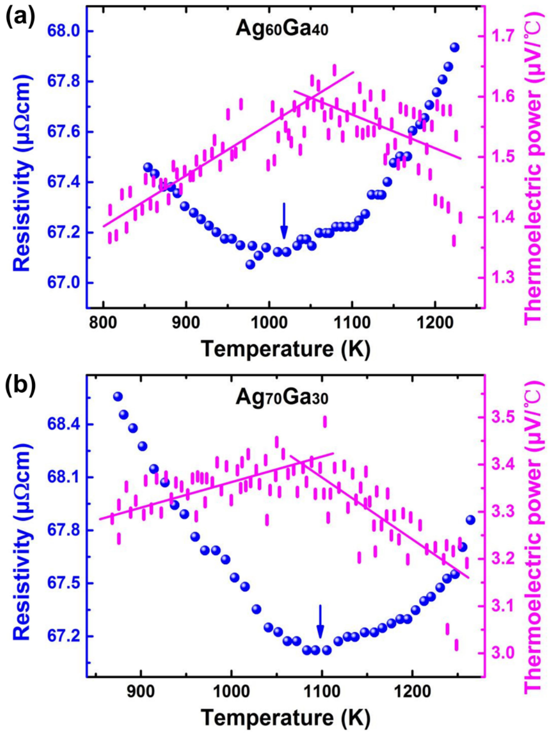

FIG. 8. The reported electrical resistivity and thermoelectric power of liquid (a) $Ag_{60}Ga_{40}$ and (b) $Ag_{70}Ga_{30}$ alloys, respectively, as a function of temperature [24].

$$\mathrm{D} = \lim_{t\to\infty} \frac{\langle |r_i(t) - r_0(t)|^2 \rangle}{6t} \tag{3}$$

where $r_i(t)$ and $r_0(t)$ are the atomic positions of atom i at time t and the initial time, respectively. Within the error bars, one can clearly reveal that no matter for the averaged, Ag or Ga atoms in liquid $Ag_{60}Ga_{40}$ alloy, kinks at about 1000 ∼ 1100 K are clearly observed. With the increase of the temperature, the activation energies of about 13.7 kJ/mol for Ag atoms and 14.1 kJ/mol for Ga atoms in the lower temperature region (below 1000 K) change to 19.5 kJ/mol for Ag atoms and 20.8 kJ/mol for Ga atoms in the higher temperature region (above 1100 K), respectively. Surprisingly, the activation energies for Ag and Ga atoms in the temperature range above 1100 K are found to be higher than those in the temperature range below 1000 K, which is in contrast to the common sense that for a uniform liquid system, the activation energy at high temperatures should be lower than that at low temperatures, indicating the existence of a structural crossover in liquid $Ag_{60}Ga_{40}$ alloy at about 1000 ∼ 1100 K. Figure 7(b) illustrates the self-diffusion coefficients of the averaged, Ag and Ga atoms in liquid $Ag_{70}Ga_{30}$ alloy as a function of temperature, in which kinks at about 1100 K are clearly observed, as guided by the trend lines. The activation energies for Ag and Ga atoms in the temperature range below 1100 K are estimated to be about 17.3 and 18.2 kJ/mol, respectively, which rise to be about 21.5 and 22.6 kJ/mol, respectively, in the temperature range above 1100 K. This phenomenon is also in contrast to the common sense for a uniform liquid system, indicating the existence of a structural crossover in liquid $Ag_{70}Ga_{30}$ alloy at about 1100 K. In addition, Figs. 8(a) and 8(b) depict the reported data of the temperature-dependent electrical resistivity (blue spheres) and thermoelectric power (magenta sticks) for liquid $Ag_{60}Ga_{40}$ and $Ag_{70}Ga_{30}$ alloys, respectively [24]. Clear minima are observed on the temperature-dependent electrical resistivity of both Ag-Ga liquids at about 1050 $\sim$ 1100 ($\pm$50) K, which are consistent with the sudden kinks on the evolutions of the thermoelectric power, as guided by the trend lines in Figs. 8(a) and 8(b). These results of the temperature-dependent electrical resistivity and thermoelectric power corroborate our structural and dynamical results well, strongly suggesting the existence of a liquid-to-liquid crossover at about 1050 $\sim$ 1100 ($\pm$50) K in both liquid $Ag_{60}Ga_{40}$ and $Ag_{70}Ga_{30}$ alloys in terms of local atomic-packing structures and properties.

IV. CONCLUSIONS

The structural evolutions of liquid $Ag_{60}Ga_{40}$ and $Ag_{70}Ga_{30}$ alloys with temperature in a range of 850 $\sim$ 1320 K have been studied by *in situ* HEXRD experiments and AIMD simulations. Experimental results, i.e., temperature-dependent peak positions of the first two peaks on $S(q)$ and $G(r)$ curves and the nearest-neighboring CN, reveal an intriguing structural change in both liquid $Ag_{60}Ga_{40}$ and $Ag_{70}Ga_{30}$ alloys at the temperature range of about 1050 $\sim$ 1100 ($\pm$50) K, which is reversible during the heating and cooling procedures. AIMD simulations reproduce the experimental observations. The temperature-dependent total CNs of both Ag-Ga liquids deviate from the linear feature at about 1000 $\sim$ 1100 K, and in the higher temperature range above 1100 K, partial $CN_{\text{Ag-Ga}}$ and $CN_{\text{Ga-Ag}}$ show an accelerated decrease while partial $CN_{\text{Ag-Ag}}$ and $CN_{\text{Ga-Ga}}$ appears to decrease much more slowly, indicating a rearrangement of Ag and Ga atoms in both Ag-Ga liquids, e.g., Ag and Ga atoms prefer to associate with themselves at higher temperatures, which can be confirmed by the temperature-dependent evolutions of Ga-Ga dimers in both Ag-Ga liquids. Meanwhile, abnormal temperature-dependent behaviors of the atomic diffusivity, electrical resistivity, and absolute thermoelectric power in both Ag-Ga liquids at about 1050 $\sim$ 1100 ($\pm$50) K further support the existence of a liquid-to-liquid crossover in both liquid $Ag_{60}Ga_{40}$ and $Ag_{70}Ga_{30}$ alloys. All results obtained here will promote the understanding of the structural evolutions in noble-polyvalent metallic melts in particular and metallic liquids in general.

ACKNOWLEDGMENTS

Financial support from the National Natural Science Foundation of China (Grants No. U1832203, No. 11975202, No. 51671169, and No. 51671170), National Key Research and Development Program of China (Grants No. 2016YFB0701203, No. 2016YFB0700201, and No. 2017YFA0403400), Natural Science Foundation of Zhejiang Province (Grants No. LY15E010003 and No. LZ20E010002), and the Fundamental Research Funds for the Central Universities is gratefully acknowledged. The *in situ* HEXRD experiments at 11-ID-C beamline, APS, Chicago and the computer resources at National Supercomputer Centers in Tianjin are also gratefully acknowledged.

---

[1] A. Cadien, Q. Y. Hu, Y. Meng, Y. Q. Cheng, M. W. Chen, J. F. Shu, H. K. Mao, and H. W. Sheng, Phys. Rev. Lett. **110**, 125503 (2013).

[2] V. V. Brazhkin, S. V. Popova, and R.N. Voloshin, High Pressure Res. **15**, 267 (1997).

[3] L. H. Xiong, X. D. Wang, Q. Yu, H. Zhang, F. Zhang, Y. Sun, Q. P. Cao, H. L. Xie, T. Q. Xiao, D. X. Zhang, C. Z. Wang, K. M. Ho, Y. Ren, and J. Z. Jiang, Acta Mater. **128**, 304 (2017).

[4] N. Funamori and K. Tsuji, Phys. Rev. Lett. **88**, 255508 (2002).

[5] F. A. Gorelli, S. D. Panfilis, T. Bryk, L. Ulivi, G. Garbarino, P. Parisiades, and M. Santoro, J. Phys. Chem. Lett. **9**, 2909 (2018).

[6] Q. Yu, X. D. Wang, Y. Su, Q. P. Cao, Y. Ren, D. X. Zhang, and J. Z. Jiang, Phys. Rev. B **95**, 224203 (2017).

[7] F. Q. Zu, X. F. Li, L. J. Guo, H. Yang, X. B. Qin, and Z. G. Zhu, Phys. Lett. A **324**, 472 (2004).

[8] C. S. Liu, G. X. Li, Y. F. Liang, and A. Q. Wu, Phys. Rev. B **71**, 064204 (2005).

[9] X. Chen, Q. Yu, Y. Su, X. D. Wang, Q. P. Cao, D. X. Zhang, and J. Z. Jiang, Scr. Mater. **148**, 68 (2018).

[10] F. Q. Zu, Z. G. Zhu, L. J. Guo, B. Zhang, J. P. Shui, and C. S. Liu, Phys. Rev. B **64**, 180203(R) (2001).

[11] W. Xu, M. T. Sandor, Y. Yu, H. Ke, H. Zhang, M. Li, W. Wang, L. Liu, and Y. Wu, Nat. Commun. **6**, 7696 (2015).

[12] S. Lan, Y. Ren, X. Y. Wei, B. Wang, E. P. Gilbert, T. Shibayama, S. Watanabe, M. Ohnuma, and X. L. Wang, Nat. Commun. **8**, 14679 (2017).

[13] S. Wei, F. Yang, J. Bednarcik, I. Kaban, O. Shuleshova, A. Meyer, and R. Busch, Nat. Commun. **4**, 2083 (2013).

[14] P. Terzieff, Phys. Chem. Liq. **41**, 431 (2003).

[15] P. Terzieff and Y. Tsuchiya, J. Phys.: Condens. Matter **13**, 3573 (2001).

[16] P. Terzieff, K. L. Komarek, and E. Wachtel, J. Phys. F: Met. Phys. **16**, 1071 (1986).

[17] Y. Arai, Y. Shirakawa, S. Tamaki, and M. Azuma, J. Phys. Soc. Jpn. **64**, 2594 (1995).

[18] G. J. Qi, M. Hino, and T. Azakami, Mater. Trans. JIM **30**, 575 (1989).

[19] L. H. Xiong, K. Chen, F. S. Ke, H. B. Lou, G. Q. Yue, B. Shen, F. Dong, S. Y. Wang, L. Y. Chen, C. Z. Wang, K. M. Ho, X. D. Wang, L. H. Lai, H. L. Xie, T. Q. Xiao, and J. Z. Jiang, Acta Mater. **92**, 109 (2015).

[20] D. Jendrzejczyk and K. Fitzner, Thermochim. Acta **433**, 66 (2005).

[21] A. K. Jena and T. R. Ramachandran, Metall. Trans. **2**, 2958 (1971).

[22] K. Wasai, M. Kano, and K. Mukai, Int. J. Thermophys. **16**, 831 (1995).

[23] R. Venkatesh and R. K. Mishra, J. Non-Cryst. Solids **351**, 705 (2005).

[24] J. Vinckel, J. Hugel, and J. G. Gasser, Philos. Mag. B **73**, 231 (1996).

[25] Y. Shirakawa, Y. Arai, T. Iida, and S. Tamaki, Thermochim. Acta **314**, 291 (1998).

[26] I. Kaban and W. Hoyer, J. Non-Cryst. Solids **312**, 41 (2002).

[27] A. P. Hammersley, S. O. Svensson, M. Hanfland, A. N. Fitch, and D. Hausermann, High Pressure Res. **14**, 235 (1996).

[28] P. Juhás, T. Davis, C. L. Farrow, and S. J. L. Billinge, J. Appl. Crystallogr. **46**, 560 (2013).

[29] B. H. Toby and R. B. V. Dreele, J. Appl. Crystallogr. **46**, 544 (2013).

[30] G. Kresse and J. Furthmüller, Comput. Mater. Sci. **6**, 15 (1996).

[31] G. Kresse and J. Hafner, Phys. Rev. B.: Condens. Matter **48**, 13115 (1993).

[32] D. X. Zhang, B. Shen, Y. X. Zheng, S. Y. Wang, J. B. Zhang, S. D. Yang, R. J. Zhang, L. Y. Chen, C. Z. Wang, and K. M. Ho, Appl. Phys. Lett. **104**, 121907 (2014).

[33] M. Zhu, M. J. Xia, F. Rao, X. B. Li, L. C. Wu, X. L. Ji, S. L. Lv, Z. T. Song, S. L. Feng, H. B. Sun, and S. B. Zhang, Nat. Commun. **5**, 4086 (2014).

[34] H. Zhang, S. L. Shang, W. Y. Wang, Y. Wang, X. D. Hui, L. Q. Chen, and Z. K. Liu, Comput. Mater. Sci. **89**, 242 (2014).

[35] S. Nosé, J. Chem. Phys. **81**, 511 (1984).

[36] W. G. Hoover, Phys. Rev. A **31**, 1695 (1985).

[37] P. E. Blöchl, Phys. Rev. B **50**, 17953 (1994).

[38] G. Kresse and J. Furthmüller, Phys. Rev. B **54**, 11169 (1996).

[39] See Supplemental Material at http://link.aps.org/supplemental/10.1103/PhysRevB.102.224103 for the MSD data of both Ag-Ga liquids, the temperature-dependent evolutions of the first peaks of experimental $S(q)$ and $G(r)$ curves derived by taking the maxima directly, and the high-quality RDF curves of both Ag-Ga liquids during the heating procedure.

[40] Y. Zhang, J. B. Li, J. K. Liang, Q. L. Liu, Y. G. Xiao, Q. Zhang, G. H. Rao, and C. R. Li, Calphad **30**, 316 (2006).

[41] W. B. Zhang, X. D. Wang, Q. P. Cao, D. X. Zhang, and J. Z. Jiang, J. Phys. Chem. B **123**, 7055 (2019).

[42] Y. Su, X. D. Wang, P. F. An, J. Zhang, T. D. Hu, Y. Ren, Q. Tao, Q. P. Cao, D. X. Zhang, and J. Z. Jiang, J. Phys. Chem. C **123**, 25209 (2019).

[43] N. A. Mauro, W. Fu, J. C. Bendert, Y. Q. Cheng, E. Ma, and K. F. Kelton, J. Chem. Phys. **137**, 044501 (2012).

[44] N. A. Mauro, V. Wessels, J. C. Bendert, S. Klein, A. K. Gangopadhyay, M. J. Kramer, S. G. Hao, G. E. Rustan, A. Kreyssig, A. I. Goldman, and K. F. Kelton, Phys. Rev. B **83**, 184109 (2011).

[45] K. Zhang, X. F. Bian, L. Yang, and Y. W. Bai, Physica B **407**, 2141 (2012).

[46] F. Zhang, Y. Sun, Z. Ye, Y. Zhang, C. Z. Wang, M. I. Mendelev, R. T. Ott, M. J. Kramer, Z. J. Ding, and K. M. Ho, J. Phys.: Condens. Matter **27**, 205701 (2015).

[47] Y. Su, X. D. Wang, Q. P. Cao, D. X. Zhang, and J. Z. Jiang, J. Phys. Chem. C **124**, 19817 (2020).

[48] O. Gross, N. Neuber, A. Kuball, B. Bochtler, S. Hechler, M. Frey, and R. Busch, Commun. Phys. **2**, 83 (2019).

[49] S. Lan, M. Blodgett, K. F. Kelton, J. L. Ma, J. Fan, and X. L. Wang, Appl. Phys. Lett. **108**, 211907 (2016).

[50] H. B. Lou, X. D. Wang, Q. P. Cao, D. X. Zhang, J. Zhang, T. D. Hu, H. K. Mao, and J. Z. Jiang, Proc. Natl. Acad. Sci. **110**, 10068 (2013).

[51] J. Ding, E. Ma, M. Asta, and R. O. Ritchie, Sci. Rep. **5**, 17429 (2015).

[52] S. P. Pan, J. Y. Qin, W. M. Wang, and T. K. Gu, Phys. Rev. B **84**, 092201 (2011).

[53] A. Pasturel, E. S. Tasci, M. H. F. Sluiter, and N. Jakse, Phys. Rev. B **81**, 140202(R) (2010).

[54] A. Pasturel and N. Jakes, Phys. Rev. B **84**, 134201 (2011).

[55] S. A. Khan, X. D. Wang, A. S. Ahmad, Q. P. Cao, D. X. Zhang, Y. Z. Fang, H. Wang, and J. Z. Jiang, J. Phys. Chem. C **123**, 20342 (2019).

[56] W. B. Zhang, X. D. Wang, Q. P. Cao, D. X. Zhang, H.-J. Fecht, and J. Z. Jiang, J. Phys.: Condens. Matter **30**, 365401 (2018).

[57] S. A. Khan, X. D. Wang, Q. P. Cao, D. X. Zhang, and J. Z. Jiang, Acta Mater. **140**, 31 (2017).

[58] L. H. Xiong, X. D. Wang, Q. P. Cao, D. X. Zhang, H. L. Xie, T. Q. Xiao, and J. Z. Jiang, J. Phys.: Condens. Matter **29**, 035101 (2017).

[59] H. B. Lou, L. H. Xiong, A. S. Ahmad, A. G. Li, K. Yang, K. Glazyrin, H. P. Liermann, H. Franz, X. D. Wang, Q. P. Cao, D. X. Zhang, and J. Z. Jiang, Acta Mater. **81**, 420 (2014).

[60] J. L. Finney, Proc. Roy. Soc. Lond. A **319**, 479 (1970).

[61] J. L. Finney, Nature (London) **266**, 309 (1977).

[62] D. Jendrzejczyk-Handzlik and K. Fitzner, J. Chem. Thermodyn. **43**, 392 (2011).

[63] X. G. Gong, G. L. Chiarotti, M. Parrinello, and E. Tosatti, Europhys. Lett. **21**, 469 (1993).

[64] K. H. Tsai, T. M. Wu, and S. F. Tsay, J. Chem. Phys. **132**, 034502 (2010).